Formation of contact and multiple cyclic cassiterite twins in SnO$_2$-based ceramics co-doped with cobalt and niobium oxides

Nina Daneu,[a]* Goran Dražič,[b] Matjaž Mazaj,[c] Fabrice Barou[d] and José Alberto Padrón-Navarta[d,e]

[a]Advanced Materials Department, Jožef Stefan Institute, Jamova cesta 39, Ljubljana, 1290, Slovenia, [b]Materials Chemistry, National Institute of Chemistry, Hajdrihova 19, Ljubljana, Slovenia, [c]Inorganic Chemistry and Technology, National Institute of Chemistry, Hajdrihova 19, Ljubljana, Slovenia, [d]Géosciences Montpellier, Université de Montpellier and CNRS, UMR5243, Montpellier, France, and [e]Andalusian Institute of Earth Sciences, Spanish Research Council and University of Granada, Granada, Spain. *Correspondence e-mail: nina.daneu@ijs.si

Contact and multiple cyclic twins of cassiterite commonly form in SnO$_2$-based ceramics when SnO$_2$ is sintered with small additions of cobalt and niobium oxides (dual doping). In this work, it is shown that the formation of twins is a two-stage process that starts with epitaxial growth of SnO$_2$ on CoNb$_2$O$_6$ and Co$_4$Nb$_2$O$_9$ seeds (twin nucleation stage) and continues with the fast growth of (101) twin contacts (twin growth stage). Both secondary phases form below the temperature of enhanced densification and SnO$_2$ grain growth; CoNb$_2$O$_6$ forms at ~700°C and Co$_4$Nb$_2$O$_9$ at ~900°C. They are structurally related to the rutile-type cassiterite and can thus trigger oriented (epitaxial) growth (local recrystallization) of SnO$_2$ domains in different orientations on a single seed particle. While oriented growth of cassiterite on columbite-type CoNb$_2$O$_6$ grains can only result in the formation of contact twins, the Co$_4$Nb$_2$O$_9$ grains with a structure comparable with that of corundum represent suitable sites for the nucleation of contact and multiple cyclic twins with coplanar or alternating morphology. The twin nucleation stage is followed by fast densification accompanied by significant SnO$_2$ grain growth above 1300°C. The twin nuclei coarsen to large twinned grains as a result of the preferential and fast growth of the low-energy (101) twin contacts. The solid-state diffusion processes during densification and SnO$_2$ grain growth are controlled by the formation of point defects and result in the dissolution of the twin nuclei and the incorporation of Nb^{5+} and Co^{2+} ions into the SnO$_2$ matrix in the form of a solid solution. In this process, the twin nuclei are erased and their role in the formation of twins is shown only by irregular segregation of Co and Nb to the twin boundaries and inside the cassiterite grains, and Co,Nb-enrichment in the cyclic twin cores.

1. Introduction

Understanding the formation of twins during crystal growth, *i.e.* growth twins is one of the fundamental challenges in mineralogy and materials science that remains incompletely understood (Shahani & Voorhees, 2016). The presence of growth twins influences the crystal morphology via the development of reentrant angles and, it is commonly observed that growth twins are larger than untwinned crystals due to their faster growth along the twin boundary planes (Shahani & Voorhees, 2016; Otálora & García-Ruiz, 2014). Both effects suggest that growth twins have the potential to be exploited for the fabrication of materials with tailored properties via controlling the crystal shape and size. Therefore, it is important to understand the process of growth twinning in detail.
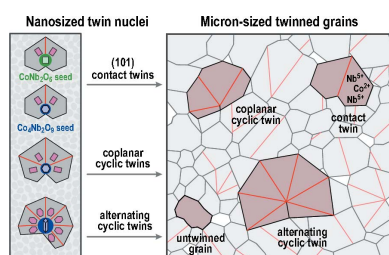
This work addresses the origin of contact and multiple cyclic twins of cassiterite (SnO_2) that form in polycrystalline SnO_2-based ceramics when SnO_2 is sintered with small amounts of cobalt oxide and niobium oxide (dual-doped SnO_2). The typical microstructure of SnO_2 with the addition of 1 mol% of CoO and 1 mol% of Nb_2O_5 after sintering at 1430°C for 5 h is shown in Fig. 1(a). In our previous studies, we described microstructure development and electrical properties of the ceramics (Tominc et al., 2018), and analyzed the morphology of multiple twins using electron back-scatter diffraction (EBSD) (Padrón-Navarta et al., 2020). We have shown that small addition of both aliovalent dopants in the Co:Nb ratio of up to 1:2 is necessary for efficient densification of the ceramics and growth of SnO_2 grains (Tominc et al., 2018). We also observed that dual doping results in the abundant formation of (101) twin boundaries (TBs) in cassiterite grains during SnO_2 grain growth (Tominc et al., 2018; Padrón-Navarta et al., 2020). Grains with a single (101) TB or contact twins are the most common among the twinned grains, whereas multiple cyclic twins represent only around 6% of all grains. Cyclic twins of two types were identified by EBSD, coplanar and alternating, both types occur in similar fractions and are randomly distributed in the microstructure.

Multiple twins are frequently observed in rutile (TiO_2) and cassiterite. The minerals are isostructural and are characterized by the $4/m\,2/m\,2/m$ point group, which has four equivalent {101} reflection planes and each can represent a twin contact. This may lead to the formation of subsequent multiple twins with a variety of morphologies (see chapter 3.3.6.9. in Hahn & Klapper, 2006). In this work, we focus on a special type of multiple twins, i.e. the cyclic twins, in which all TBs radiate from a common twin core. Both types of cyclic twins, with coplanar and alternating morphology, can be derived from a contact (101) twin as schematically shown in Figs. 1(b)–1(d). Fig. 1(b) is a $(101)_{Cst}$ contact twin oriented along the $[010]_{Cst}$ and $[111]_{Cst}$ zone axes common to both twin domains. In every orientation, two sets of $\{101\}_{Cst}$ reflection planes are edge-on oriented (in each twin domain), and the other $\{101\}_{Cst}$ reflection planes are oblique to the viewing direction. Cyclic twins form when twin contacts develop on subsequent edge-on oriented {101} reflection planes with all domains aligned along the same zone axis. In coplanar cyclic twins, the twin domains have the $[010]_{Cst}$ axis in common [Fig. 1(c)], whereas, in alternating cyclic twins, all twin domains are oriented along their $[111]_{Cst}$ zone axis [Fig. 1(d)]. A more detailed description of both types of multiple cyclic twins of cassiterite that occur in the dual-doped SnO_2 is given by Padrón-Navarta et al. (2020).

Twins of different morphology and origin have been described in synthetic SnO_2. Deformation twins on {101} planes can be introduced into SnO_2 (and also in isostructural rutile, TiO_2) crystals by mechanical grinding (Suzuki et al., 1991). Twinning during crystal growth was also reported; for example, contact, polysynthetic, and cyclic growth twins on {101} planes were found in nanocrystalline SnO_2 thin films produced from amorphous oxygen-deficient SnO_2 indicating
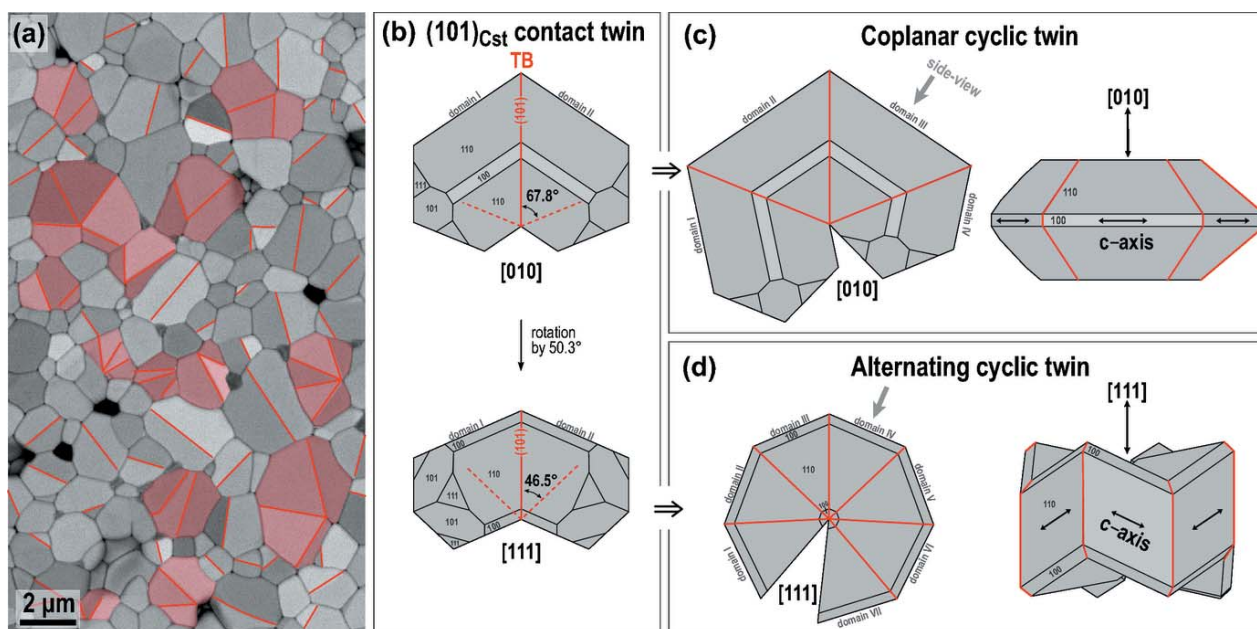
Figure 1
(a) Typical microstructure of cobalt and niobium oxide-doped SnO_2-based ceramics composed of cassiterite (SnO_2) grains that frequently contain (101) twin boundaries (TBs; marked by red lines). Most grains are untwinned, some contain a single TB, these are contact (101) twins, and some grains contain two or more TBs, these are multiple cyclic twins (shaded in red). (b) A $(101)_{Cst}$ contact twin viewed along the $[010]_{Cst}$ and $[111]_{Cst}$ common zone axis. Dashed red lines indicate edge-on oriented $\{101\}_{Cst}$ reflection planes in the twin domains. (c) Coplanar cyclic twin of cassiterite with four domains viewed along the common $[010]_{Cst}$ axis. The side-view reveals that the tetragonal c axes of all domains lie in the same plane. (d) Alternating cyclic twins of cassiterite contain up to seven domains (see Padrón-Navarta et al. (2020) for detailed description) oriented along their $[111]_{Cst}$ zone axes. In this type of cyclic twins, the c axes of twin domains alternate up and down as visible in the side view of the twin.

the role of nonstoichiometry in the twinning process (Zheng *et al.*, 1996). Abundant {101} twins in epitaxial thin films of SnO_2 produced from α-SnO precursor on ($\bar{1}012$) sapphire (Al_2O_3) substrate formed as a result of oriented growth and recrystallization of α-SnO to SnO_2 (Pan & Fu, 2001). Contact twins also formed in Cu_2O flux-grown SnO_2 crystals with the addition of trivalent (Fe^{3+}) and pentavalent (Nb^{5+}, Ta^{5+}) cations suggesting the role of these dopants in the formation of the twins (Kawamura *et al.*, 1999). In our previous work, we analyzed (101) TBs in the dual-doped SnO_2 (Tominc *et al.*, 2018) by aberration-corrected scanning transmission electron microscopy and confirmed that the concentration of Co and Nb along the TB planes is slightly increased but the distribution of both elements within the interface is not uniform (Tominc *et al.*, 2018). This indicates that these twins are not chemically induced (or impurity-induced) planar defects like, for example, basal-plane inversion boundaries in Sb-doped ZnO (Rečnik *et al.*, 2001a) or {111} twins in Be-doped $MgAl_2O_4$ spinel (Drev *et al.*, 2013). The fact that all TBs in cyclic twins radiate from a common center suggests their formation by nucleation at the beginning of crystal growth; however, the reasons for the formation of different types of cyclic twins were not revealed yet.

Twinning has been even more thoroughly investigated in isostructural rutile, TiO_2 (Rt). Here, the effect of polymorphism on the formation of twins has been identified in natural as well as in synthesized samples. Nano-scale lamellae of the high-pressure and high-temperature polymorph of TiO_2 with the α-PbO_2 structure were found at {101} TBs in rutile grains in ultrahigh-pressure metamorphic rocks (Hwang *et al.*, 2000; Meng *et al.*, 2008). Penn & Banfield (1998) have shown that oriented attachment of polymorphic TiO_2 nanoparticles can result in twinning and oriented intergrowths. Another mechanism leading to rutile crystals/domains in twinned orientation is oriented (topotaxial) recrystallization and/or epitaxial growth of/on structurally related precursor minerals (Armbruster, 1981; Force *et al.*, 1996). Oriented recrystallization of ilmenite (Ilm) $FeTiO_3$ with $[101]_{Rt}$ or $[001]_{Rt}$ parallel to $[210]_{Ilm}$ results in the formation of complex reticulated (sagenite) rutile networks composed of twin contacts on {101} and {301} planes (crystallographic contacts) or rutile domains intersecting at 60 or 120° (non-crystallographic contacts) (Rečnik *et al.*, 2015; Stanković *et al.*, 2016). In principle, oriented recrystallization can result in the development of coplanar cyclic twins of rutile, which can be theoretically composed of up to six rutile domains, separated by five {101} TBs and an additional non-crystallographic contact (Hahn & Klapper, 2006; Padrón-Navarta *et al.*, 2020). Besides coplanar cyclic twins, alternating twins with non-planar fourfold (tetragonal) *c* axes and composed of eight domains due to the 45° angle between the (101) and (01$\bar{1}$) planes (Hahn & Klapper, 2006) are also found in rutile. Well known examples of these rare natural occurrences of symmetrically developed eightlings from Magnet Cove (Arkansas, USA). According to Hahn & Klapper (2006), Magnet Cove eightlings are nucleation twins, which originate from a common point (nucleus); however, the nature of the nucleus has not been described.

While the formation of certain types of twins in rutile-type minerals is well understood, the origin of cyclic twins is still puzzling the researchers. In this work, we aim to understand the formation mechanism of different types of twins that form in SnO_2 when it is doped with cobalt and niobium oxides (Tominc *et al.*, 2018). Twins, especially the multiple cyclic twins, abundantly form only in the dual-doped SnO_2 and their morphology is typical of nucleation twinning. To confirm the origin of cyclic twins by nucleation, we first analyzed the core of a cyclic twin by scanning transmission electron microscopy (STEM). Then we studied phase relations in SnO_2 with higher additions of cobalt and niobium oxides to reveal which secondary phases that could potentially trigger the formation of cyclic twins form during the sintering. Based on the results we explain the formation mechanism of contact and cyclic twins by epitaxial recrystallization of SnO_2 on particles of two secondary phases that form during the sintering, $CoNb_2O_6$ and $Co_4Nb_2O_9$, which are both structurally related to cassiterite and describe the development of microstructures composed of normal (untwinned) grains and twins.

2. Experimental

2.1. Synthesis of samples

For our studies of core regions of cyclic twins, we used SnO_2 doped with low amounts of cobalt oxide and niobium oxide, where the formation of large and abundantly twinned cassiterite grains is observed [see microstructure in Fig. 1(*a*), and also Tominc *et al.* (2018) and Padrón-Navarta *et al.* (2020)]. The samples were prepared by the standard solid-state synthesis, where SnO_2 powder (Alfa Aesar, 99.9%, nanopowder) with the addition of 1 mol% CoO (Alfa Aesar, 95%) and 1 mol% Nb_2O_5 (Merck, 99%) was homogenized in absolute ethanol, dried and pressed into pellets. The pellets were sintered at 1430°C for 5 h in air.

For the studies of phase changes within the SnO_2–Co_3O_4–Nb_2O_5 system and to obtain a deeper insight into the role of secondary phases on the formation of twins in dual-doped cassiterite, we prepared compositions with higher additions of both oxides. Two series of samples with Co:Nb ratio for the formation of $CoNb_2O_6$ and $Co_4Nb_2O_9$ phases (Co:Nb ratio 1:2 and 2:1, respectively) were prepared. In both series we added 10, 25 and 50 mol% of Co_3O_4 (Alfa Aesar, 99.7%) and Nb_2O_5 mixture, in the ratio for the formation of the targeted cobalt–niobium oxide phase, to the SnO_2 powder. The initial compositions of all samples are given in Table 1. In preparation of these compositions, we considered only the Co:Nb ratio and disregarded the oxygen nonstoichiometry due to the addition of Co_3O_4 instead of CoO, since Co^{3+} in Co_3O_4 is reduced to Co^{2+} above 800°C (Navrotsky *et al.*, 2010). The powder mixtures were homogenized in absolute ethanol, pressed into pellets, and fired at 700, 800, 900, 1000, 1100, 1200 and 1300°C for 16 h in air. After each firing, the samples were crushed, homogenized in absolute ethanol, dried, and re-pressed into pellets for firing at higher temperature.

research papers

Table 1
Compositions for the analysis of phase changes in the SnO_2-Co_3O_4-Nb_2O_5 system.

(a) Compositions for the formation of the columbite-type $CoNb_2O_6$ phase X $(SnO_2) + (100-X) (1Co_3O_4 + 3Nb_2O_5)$; Co:Nb = 1:2; X in mol%.

SnO_2		Co_3O_4		Nb_2O_5	
X (mol%)	wt%	mol%	wt%	mol%	wt%
90	83.937	2.50	3.725	7.50	12.338
75	63.527	6.25	8.459	18.75	28.014
50	36.733	12.50	14.673	37.50	48.594

(b) Compositions for the formation of the corundum-type $Co_4Nb_2O_9$ phase $Y(SnO_2) + (100 - Y)(4Co_3O_4 + 3Nb_2O_5)$; Co:Nb = 2:1; Y in mol%.

SnO_2		Co_3O_4		Nb_2O_5	
Y (mol%)	wt%	mol%	wt%	mol%	wt%
90	84.357	5.714	8.557	4.286	7.086
75	64.254	14.286	19.556	10.714	16.190
50	37.470	28.571	34.207	21.429	28.323

2.2. Characterization techniques

Atomic scale analyses of the low-doped cassiterite ceramics were performed using aberration-corrected scanning transmission electron microscopy (STEM; ARM 200CF, Jeol Ltd, Tokyo, Japan) equipped with a high-angle annular dark-field detector (HAADF) for Z-contrast imaging and energy-dispersive X-ray spectrometer (EDXS; Jeol Centurio) with 100 mm^2 silicon drift detector for chemical analysis at the nanoscale. Samples for STEM analyses were prepared by thinning, dimpling, and Ar ion-milling to perforation (Gatan PIPS 691, California, USA).

X-ray powder diffraction (XRD) was used for the determination of the phase composition of the samples. The analyses were performed on Bruker AXS, D4 Endeavor diffractometer, within an angular range of 2Θ from 10° to 70° with a step size of 0.04° and collection time of three seconds per step. The obtained data were used for the quantification of phases by Rietveld refinement using *Topas Academic v.6* software package. The quantification refinement included the whole pattern profile fit in the first step followed by unit-cell parameters fit. Additionally, temperature parameters and cation positions were fitted for the involved structural models due to the certain degree of cation disorder expected in the sintered phases.

Densification of the samples was monitored by a hot-stage microscope (EM201x, Hesse instruments). The diameter of a cylindrical sample with initial dimensions of 8 mm diameter and 5 mm height was measured during heating with 5 K min^{-1} up to 1450°C.

EBSD analyses were performed on CamScan X500FE Crystal Probe with inclined column optimized for EBSD and field-emission electron gun allowing high-resolution spatial analyses. The EBSD patterns were recorded at 20 kV accelerating voltage and a working distance of 20 mm. The patterns were indexed automatically using the *AZtechHKL* software package from Oxford Instruments. See Padrón Navarta *et al.* (2020) for more details about the EBSD analyses.

3. Results and discussion

3.1. STEM/EDXS analysis of the cyclic twin core

The most typical morphological feature of cyclic twins of cassiterite that form in the dual-doped SnO_2-based ceramics is the common origin (nucleation point) of all TBs in cyclically twinned grains [see Fig. 1(a) and Padrón Navarta *et al.* (2020). This suggests that all TBs form on a common nucleus at the beginning of crystal growth. To find the nucleus in the twin core of cyclic twins, we analyzed the low-doped ceramics by atomic resolution STEM. The task is challenging because cyclic twins represent only about six percent of all grains (Padrón-Navarta *et al.*, 2020) and hence the probability of
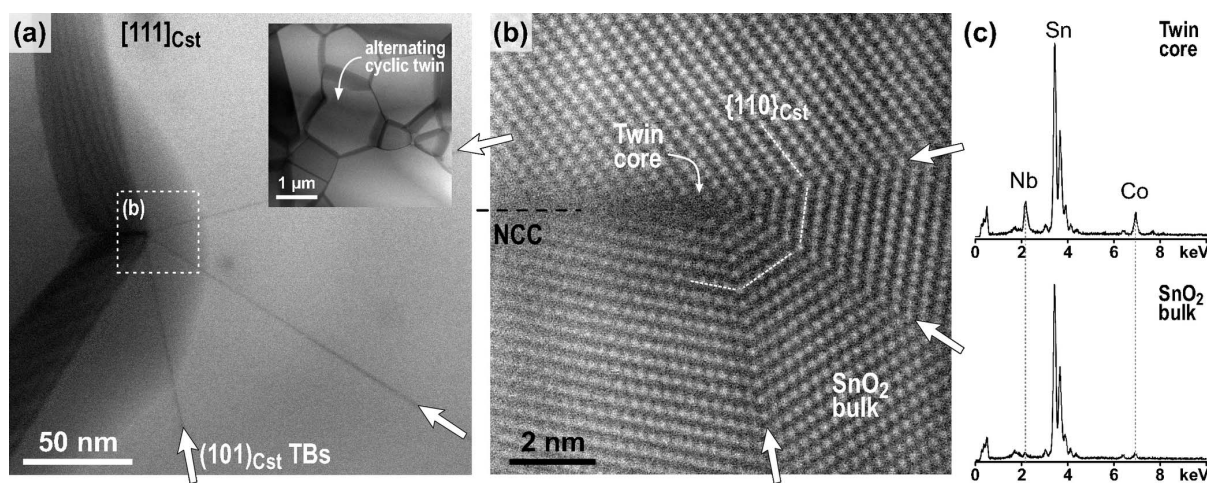
Figure 2
STEM/EDXS analysis of an alternating cyclic twin with four domains. (a) Low-magnification STEM image of the twinned grain viewed along the common [111]$_{Cst}$ zone axis. The three (101)$_{Cst}$ TBs and the NCC extend from a common point located near the edge of the grain. (b) HAADF-STEM image of the region around the core. (c) EDXS point analyses from the cyclic twin core and bulk SnO_2 indicate significant enrichment with Nb and Co in the core region.

finding a cyclic twin, which is oriented close to the common zone axis ([010] for coplanar and [111] for alternating twins), with a visible nucleation core and, at the same time, located in the thin part of the sample, is relatively low. An example of an alternating cyclic twin with four domains, located in a slightly thicker, but still electron-transparent part of the sample and oriented along the common [111] zone axis is shown in Fig. 2.

The cyclic twin contains three TBs extending from a common center, which is positioned near the edge of the grain [Fig. 2(a)]. Such eccentric position of the twin core is typical for cyclic twins in cassiterite ceramics as previously observed based on SEM and EBSD analyses (Tominc et $al.$, 2018; Padrón-Navarta et $al.$, 2020). A high-resolution HAADF-STEM image taken around the twin core region is shown in Fig. 2(b). The bright contrast stems mainly from the heavy Sn atomic columns (cation substructure) and shows that all three TBs are edge-on oriented and lie in subsequent edge-on oriented (101) planes with a 46.5° angle between two planes. At this magnification, the common origin point of all TBs of the cyclic twin is even more obvious. All three TBs are mirror-symmetric across the twin plane. This atomic configuration of the TB corresponds to the lowest-energy pseudo-twin model of {101} twins characterized by in-plane translation of $\frac{1}{2}\langle 111\rangle$ in SnO$_2$ (Lee et $al.$, 1993). In addition to the three twin boundaries (crystallographic contacts), the cyclic twin contains an additional non-crystallographic contact (NCC) between the first and the last (fourth) domain, which is incomparably shorter than the twin boundaries [Figs. 2(a) and 2(b)]. This is due to the lower degree of local atomic ordering at the NCC in comparison to crystallographic contacts like twin boundaries and hence such an interface is not energetically favored. The core region contains no visible secondary crystalline phase and can be described as a nanosized amorphous pocket [Fig. 2(b)]. EDXS spectra were recorded in bulk SnO$_2$ and in the core [Fig. 2(c)]. While bulk SnO$_2$ contains only low amounts of Co and Nb in the form of solid solubility, the amorphous core region is significantly enriched in Co and Nb. Quantification of EDXS spectra was unreliable due to the relatively large thickness at the area of interest, low count ratio, and inconvenient sample tilt relative to the detector. EDXS analysis was performed also on the TBs, where segregation of Co or Nb was not detected by EDXS, however previous analyses of this sample using quantitative HAADF-STEM indicated low and nonuniform segregation of Co and Nb to the TB planes (Tominc et $al.$, 2018).

Excess of Co and Nb detected in the core of the cyclic twin, however, does suggest the presence of a Co- and Nb-rich precursor phase during the nucleation stage. The question is why there is no crystalline Co–Nb phase in the core. One of the possible explanations is that the cross-section did not exactly intersect the nucleus, which has been located above or below the thin section. Another possibility is that a seed particle existed before the growth of the cyclic twin when it served as a twin nucleation core, and later, in the process of SnO$_2$ crystal growth at higher temperatures, it reacted with SnO$_2$ causing the incorporation of Co and Nb in the bulk cassiterite in the form of solid solution. This process is even more likely in the samples with low doping rates, where the addition of both dopants does not exceed the solid solubility limits of Co and Nb in SnO$_2$ (the estimated value of total Co and Nb solid solubility in SnO$_2$ is around 4–6 at%) and therefore most of the Co and Nb is incorporated into SnO$_2$ in the ~1:2 to 1:4 ratio. The total amount of Co and Nb and the Co:Nb ratio vary within these limits inside the SnO$_2$ grains, whereas excess cobalt oxide reacts with SnO$_2$ to Co$_2$SnO$_4$ spinel grains (Tominc et $al.$, 2018).

The fact that cyclic twins are observed only in the samples with the addition of both aliovalent oxides (cobalt and niobium oxide) is a strong indication that the nucleation of cyclic twins is related to the formation of a cobalt–niobium oxide. The formation of such a secondary phase in the form of nanosized nuclei and its transient stability is another possible scenario of twin formation, and would agree with the theory about the formation of cyclic twins by nucleation proposed by Senechal (1980). To check the hypothesis we prepared SnO$_2$ samples with higher additions of Co$_3$O$_4$ and Nb$_2$O$_5$ and investigated which phases form during the heating and how they relate to twinning in cassiterite.

3.2. Phases in SnO$_2$ with higher additions of Co$_3$O$_4$ and Nb$_2$O$_5$

According to the literature, CoNb$_2$O$_6$, Co$_3$Nb$_4$O$_{14}$, and Co$_4$Nb$_2$O$_9$ are cobalt–niobium oxides that form during the sintering of CoO–Nb$_2$O$_5$ in air (Goldschmidt, 1960; Weitzel, 1976; Castellanos et $al.$, 2006). CoNb$_2$O$_6$ crystallizes in the columbite-type structure (abbreviated as Col-t[1]), the structure of Co$_3$Nb$_4$O$_{14}$ is comparable to that of rutile, and the structure of Co$_4$Nb$_2$O$_9$ is comparable to that of corundum (we use abbreviation Crn-t for this phase). CoNb$_2$O$_6$ and Co$_4$Nb$_2$O$_9$ are both interesting in connection with nucleation twinning in cassiterite. We first synthesized both phases from stoichiometric amounts of initial oxides (Co$_3$O$_4$ and Nb$_2$O$_5$, taking into account the Co:Nb atomic ratio) at 1200°C (results not shown here). To follow phase changes in the SnO$_2$–Co$_3$O$_4$–Nb$_2$O$_5$ system with increasing temperature, we studied compositions that contained 10, 25 and 50 mol% of Co$_3$O$_4$ and Nb$_2$O$_5$ in the ratio for the formation of CoNb$_2$O$_6$ and Co$_4$Nb$_2$O$_9$ (Co:Nb ratios 1:2 and 2:1, see Table 1). Here we show only the results of XRD analyses for the samples with 50 mol% of both dopant mixtures because in these samples the phase changes are best visible due to the high addition of both oxides. The XRD patterns are shown in Fig. S1. XRD patterns of the samples with 10 and 25 mol% are similar, only the amount of secondary phases is lower. The phase composition of the samples with 50 mol% addition of the dopants mixture after firing at each temperature was quantified using the Rietveld refinement procedure and the results are shown in Figs. 3(a) and 3(b).

In the sample with the addition of cobalt and niobium oxides with Co:Nb ratio 1:2 [Fig. 3(a)], the CoNb$_2$O$_6$ phase starts to form already below 700°C. The reaction is completed

---

[1] Abbreviation for columbite is not in the list of Whitney & Evans (2010); we decided to use Col.

Nina Daneu et $al.$ · Multiple cyclic cassiterite twins in SnO$_2$-based ceramics
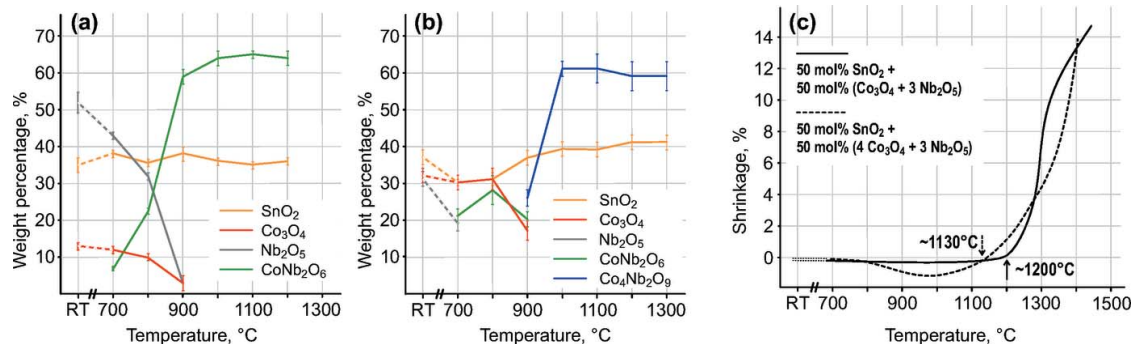
Figure 3
Phase changes during firing of SnO$_2$ with the addition of 50 mol% of Co$_3$O$_4$ and Nb$_2$O$_5$ in the ratio for the formation of (a) CoNb$_2$O$_6$ phase and (b) Co$_4$Nb$_2$O$_9$ phase. (c) Densification curves of both compositions.

at 1000°C, when reflections from the starting oxides Co$_3$O$_4$ and Nb$_2$O$_5$ are not observed anymore and only reflections from rutile-type SnO$_2$ and CoNb$_2$O$_6$ are present. The two phases coexist up to 1200°C. After sintering at 1300°C, the reflections from both phases almost completely disappear (a small amount of SnO$_2$ remains unreacted) and a new phase is formed. Reflections of this phase could not be matched with any phase in the available databases. Preliminary analyses with SEM/EDXS have shown that the phase has an approximate composition of SnCoNb$_2$O$_8$ and according to the XRD pattern, it has a similar structure to the low-temperature form of FeNb$_2$O$_6$, which has the trirutile structure (Aruga et al., 1985; Beck, 2012). This suggests that the columbite-type CoNb$_2$O$_6$ phase reacts with SnO$_2$ above 1200°C to form a structurally similar quaternary oxide.

In the second series of compositions, the Co$_3$O$_4$ and Nb$_2$O$_5$ were added to SnO$_2$ in the ratio for the formation of Co$_4$Nb$_2$O$_9$ phase (Co:Nb = 2:1). The results of Rietveld analysis of XRD patterns are shown in Fig. 3(b). Also here, the columbite-type CoNb$_2$O$_6$ is the first secondary phase that forms in the system already below 700°C. The fraction of this phase increases at 800°C; however, at 900°C its amount starts to decrease and reflections of the Co$_4$Nb$_2$O$_9$ phase (Bertaut et al., 1961) appear as a result of the reaction between CoNb$_2$O$_6$ and the remaining cobalt oxide. After sintering at 1000°C, only SnO$_2$ and Co$_4$Nb$_2$O$_9$ are present in the sample and their amount is stable up to 1300°C (after sintering at 1400°C, the sample with the highest addition of Co and Nb-oxide melted). SEM/EDXS analysis has shown around 3–4 at% Sn in Co$_4$Nb$_2$O$_9$ and 4–6 at% of Co and Nb in 1:2 ratio in cassiterite grains in all samples, therefore these values are the approximate (estimated) solid solubility limits.

In ceramics, grain growth is closely related to diffusion processes and accelerated shrinkage. Densification characteristics of both compositions are shown in Fig. 3(c) and indicate that both compositions start to densify above 1100°C. In SnO$_2$-based ceramics with lower additions of both dopants, the onset of densification is shifted even to temperatures above 1300°C (Tominc et al., 2018). These temperatures are much higher than the formation of cobalt niobium oxides and indicate that SnO$_2$ grain growth occurs much after the formation of both secondary phases.

The sample with 50% addition of Co$_3$O$_4$ and Nb$_2$O$_5$ in the ratio for the formation of Co$_4$Nb$_2$O$_9$ phase after sintering at 1300°C was analyzed by EBSD, and the sample with 10% addition of both dopants in the same ratio was inspected by TEM. Fig. 4(a) is EBSD phase map of the sample showing grains of the two identified phases, SnO$_2$ and Co$_4$Nb$_2$O$_9$ in blue and brown, respectively. The grain misorientation analysis has confirmed the presence of (101) twin boundaries in cassiterite grains. Interestingly, cyclic twins, especially those with more than three subsequent domains are quite rare in this sample in comparison to the low-doped ceramics (Tominc et al., 2018; Padrón-Navarta et al., 2020). This suggests that the conditions for the formation of cyclic twins are more easily fulfilled in samples with lower dopant additions. EBSD data was further used for the analysis of the orientation relationship (OR) between cassiterite and Co$_4$Nb$_2$O$_9$ grains. The misorientation angle analysis of the SnO$_2$–Co$_4$Nb$_2$O$_9$ contacts [Fig. 4(a)] reveals that certain orientations between the two phases occur with the probability that is above the uniform misorientation distribution function (MDF) indicating preferential formation of correlated orientation relationship between grains of these two phases. The analysis of the misorientation data using MTEX toolbox (Hielscher & Schaeben, 2008; Mainprice et al., 2015; Krakow et al., 2017; Grimmer, 1979; Morawiec, 1997) has shown that these misorientations are crystallographic contacts that follow the OR: (101)$_{Cst}$ || (110)$_{Crn-t}$ and (010)$_{Cst}$ || (001)$_{Crn-t}$. In Fig. 4(a), these contacts are marked by red lines. Epitaxial OR between SnO$_2$ and Co$_4$Nb$_2$O$_9$ was also found in TEM. Fig. 4(b) shows a contact between a larger SnO$_2$ grain and a smaller Co$_4$Nb$_2$O$_9$ particle. The cassiterite grain is oriented along the [111]$_{Cst}$ zone axis, while the Co$_4$Nb$_2$O$_9$ grain along the pseudocubic [$\bar{2}$21]$_{Crn-t}$ zone axis with (101)$_{Cst}$ planes parallel to the (110)$_{Crn-t}$ planes of Co$_4$Nb$_2$O$_9$. This OR is equivalent to the one determined by EBSD and confirms that cassiterite grains preferentially from this type of epitaxial contact with Co$_4$Nb$_2$O$_9$.

Our studies of phase formation during the sintering of SnO$_2$ with high additions of cobalt oxide and niobium oxide (much above the solid solubility limit of Co and Nb in SnO$_2$) have shown that two secondary phases form in the system; the columbite-type CoNb$_2$O$_6$ and Co$_4$Nb$_2$O$_9$. While CoNb$_2$O$_6$ is

only a transient phase that reacts with SnO_2 above 1200°C, the results of EBSD and TEM analyses revealed that larger grains of the $Co_4Nb_2O_9$ phase remain stable up to 1300°C. SnO_2 grains start to coarsen above the $Co_4Nb_2O_9$ formation temperature and frequently develop epitaxial OR with the $Co_4Nb_2O_9$ grains. Although these phases were not detected in the low-doped ceramics (Tominc et al., 2018), it may be anticipated that they do form also in the low-doped samples in the regions of local chemical inhomogeneities during the heating and act as seeds for oriented growth of SnO_2. In the following, we explain the formation of contact and cyclic twins in the dual-doped SnO_2-based ceramics based on the structural relationship between SnO_2, $CoNb_2O_6$, and $Co_4Nb_2O_9$. Reasons for a fairly high fraction of untwinned grains in the low-doped ceramics are also discussed.

### 3.3. Twinning in SnO_2 in the presence of $CoNb_2O_6$ and $Co_4Nb_2O_9$

3.3.1. Structural relationship between SnO_2, $CoNb_2O_6$, and $Co_4Nb_2O_9$.
Both secondary phases, $CoNb_2O_6$, and $Co_4Nb_2O_9$, that form during sintering of dual-doped SnO_2 are key to constraining the twinning relations in cassiterite. Fig. 5 shows crystal structures of the three phases oriented along the zone axes that are most important for understanding the formation of contact and subsequent coplanar and alternating cyclic twins in cassiterite. The relevant structural data for the three phases are given in Table 2.

Cassiterite is structurally related to $CoNb_2O_6$ and $Co_4Nb_2O_9$ through the hexagonal close-packed (hcp) oxygen substructure. The three phases have different arrangements of the cations within the close-packed layers [Figs. 5(a)–5(c)]. In cassiterite [Fig. 5(a)], the close-packed oxygen layers are severely corrugated and extend in two directions normal to each other, i.e. along the a and b axes [the $(200)_{Cst}$ and $(020)_{Cst}$ planes] (Baur, 1981). Hence, the sixfold symmetry axis along the direction of the close-packed layers is lost and a new fourfold axis that extends along the c-axis of the structure is created (West & Bruce, 1982). The loss of the sixfold axis can be observed as a deviation of the angles between the three arrays of oxygen atoms [the $(002)_{Cst}$, $(101)_{Cst}$ and $(\bar{1}01)_{Cst}$ planes in cassiterite] within a close-packed layer from the ideal 60° [see stereogram in Fig. 5(a)]. In a close-packed layer of cassiterite, one-half of octahedral sites are occupied by Sn^{4+} cations, and these form infinite chains of edge-shared octahedra along the c-axis.

In columbite-type $CoNb_2O_6$ [Fig. 5(b)] the close-packed oxygen layers lie along the a axis, i.e. along the $(600)_{Col-t}$ planes. $CoNb_2O_6$ is structurally similar to scrutinyite (α-PbO_2), a high-temperature polymorph of PbO_2 (Weitzel, 1976). Within a single close-packed layer, the cations form a zigzag pattern of edge-shared octahedra. Co^{2+} and Nb^{5+} ions
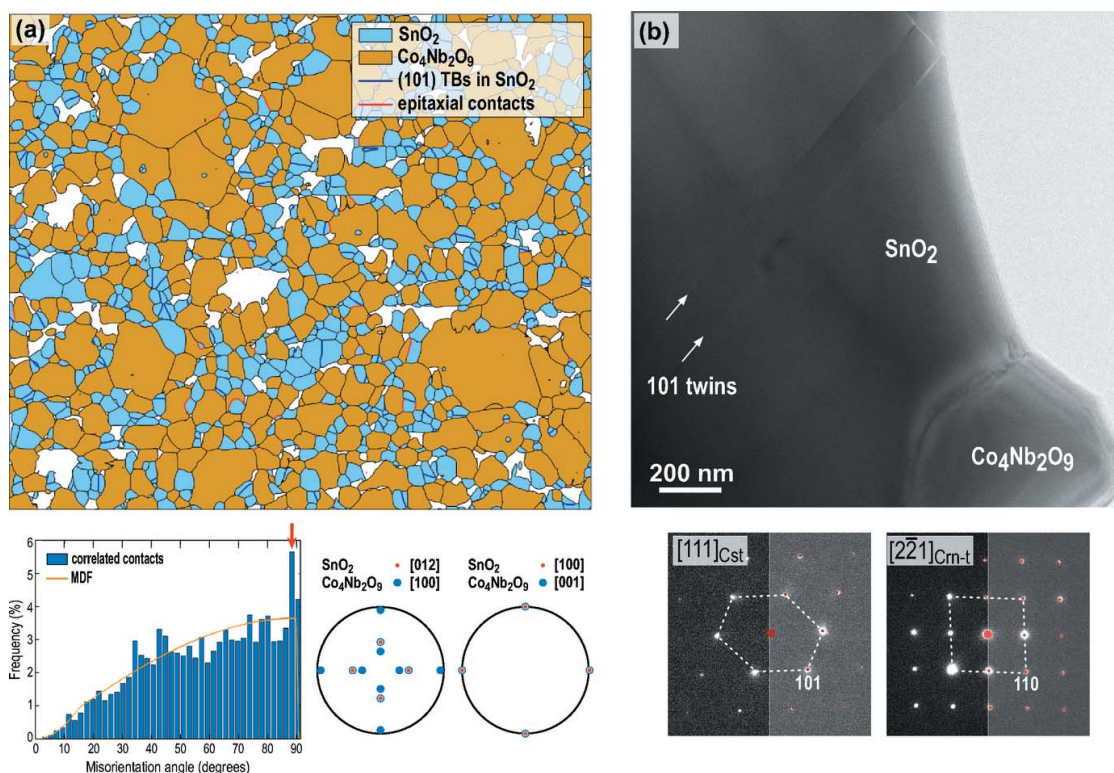
Figure 4
(a) Phase-colored EBSD map of SnO_2 with 50% addition of Co_3O_4 and Nb_2O_5 in the ratio for the formation of $Co_4Nb_2O_9$ phase sintered at 1300°C. Blue lines are (101) TBs in SnO_2 grains, whereas red lines indicate epitaxial contacts between SnO_2 (blue) and $Co_4Nb_2O_9$ (brown) with $(101)_{Cst} \parallel (110)_{Crn-t}$ and $(010)_{Cst} \parallel (001)_{Crn-t}$. The frequency of these contacts is above the uniform misorientation distribution function (MDF) as shown in the histogram below the map. (b) TEM image of the sample with the 10% addition of both oxides in the same ratio shows a SnO_2 grain in contact with $Co_4Nb_2O_9$ particle. Selected area diffraction patterns recorded from both phases disclose epitaxial OR between both phases: $[111]_{Cst}(101)_{Cst} \parallel [2\bar{2}1]_{Crn-t}$ $(110)_{Crn-t}$. This OR is identical to the epitaxial contacts determined by EBSD.

Table 2
Structural data for SnO_2, $CoNb_2O_6$ and $Co_4Nb_2O_9$ relevant for understanding the formation of contact and cyclic twins in cassiterite.

Phase	Basic structural data	Relevant lattice planes and spacings	Epitaxial relationships and lattice mismatches
SnO_2 (Cassiterite)	ICSD 84576 Tetragonal; $P4_2/mnm$ $a = 4.737$ Å $c = 3.185$ Å	$d(101)_{Cst} = 2.644$ Å $d(200)_{Cst} = 2.398$ Å	$[010]_{Cst} \parallel [100]_{Col-t}$ $(101)_{Cst} \parallel (002)_{Col-t}$; 4.7% $(101)_{Cst} \parallel (021)_{Col-t}$; 4.8% $(200)_{Cst} \parallel (021)_{Col-t}$; 6.2%
$CoNb_2O_6$	ICSD 15854 Orthorhombic; $Pbcn$ $a = 14.148$ Å $b = 5.712$ Å $c = 5.045$ Å	$d(002) = 2.522$ Å $d(021) = 2.485$ Å	--------------------------------
$Co_4Nb_2O_9$	ICSD 27134 Trigonal, $P\bar{3}c1$ $a = 5.177$ Å $c = 14.168$ Å	$d(110) = 2.589$ Å $d(102) = 3.788$ Å $d(104) = 2.776$ Å	$[010]_{Cst} \parallel [100]_{Crn-t}$ $(101)_{Cst} \parallel (110)_{Crn-t}$; 2.1% $(200)_{Cst} \parallel (110)_{Crn-t}$; 8.9% $101)_{Cst} \parallel (104)_{Crn-t}$; 4.9%

occupy subsequent layers in the 1:2 ratio; two layers are occupied by Co^{2+} and every third layer by Nb^{5+}. This causes tripling of the unit cell along the a axis. Octahedra in the neighboring close-packed layers are corner-shared. The distortion of oxygen arrays along the close-packed layers is smaller than in cassiterite, the angle between the $(021)_{Col-t}$ and $(02\bar{1})_{Col-t}$ edge-on planes is around 59°. $Co_4Nb_2O_9$ has trigonal structure comparable to that of corundum, in which two-thirds of the available octahedral interstices are occupied within the hcp oxygen substructure. Typical of the corundum-type structure is arrangement of the cations in a honeycomb pattern within a close-packed layer (Lee & Lagerlof, 1985). In $Co_4Nb_2O_9$, the Co^{2+} and Nb^{5+} occupy the octahedral interstices in 2:1 ratio on average [Fig. 5(c)]: two out of three subsequent close-packed layers have mixed composition with Co:Nb in 1:1 ratio, whereas every third layer is occupied only with Co cations, which yields overall Co:Nb ratio of 2:1. Here, oxygen atoms within the close-packed layer are symmetrically arranged and the equivalent $(110)_{Crn-t}$ attice planes intersect exactly at 60°.

Orientation of the SnO_2 and $Co_4Nb_2O_9$ in schemes of Figs. 5(a) and 5(c) is based on the results of EBSD and TEM analyses (Fig. 4) where it was confirmed that $(101)_{Cst}$ planes are parallel to $(110)_{Crn-t}$ planes. This OR is central to understanding the formation of cyclic twins in cassiterite. Another possible OR would be with the c axis of cassiterite parallel to the $\{110\}_{Crn-t}$ planes of the corundum-type phase: $[010]_{Cst} \parallel [001]_{Crn-t}$ and $(200)_{Cst} \parallel (110)_{Crn-t}$; however, no evidence for the existence of this R was found in our samples and also the high lattice mismatch between these two planes (Table 2) is not in favor to the formation of this OR. Orientation of the columbite-type $CoNb_2O_6$ phase [Fig. 5(b)] with $(101)_{Rt}[010]_{Rt} \parallel (002)_{Col-t}[100]_{Col-t}$ was selected based on the OR reported by Wittkamper et al. (2017).

The $[010]_{Cst}$ orientation [Fig. 5(a)] is important for understanding the formation of coplanar cyclic twins of cassiterite, where all twin domains are oriented along a common $[010]_{Cst}$ zone axis, whereas the $[\bar{1}11]_{Cst}$ zone axis [Fig. 5(d)] is relevant for studying alternating cyclic twins, where all twin domains have the $[111]_{Cst}$ axis in common. The two orientations are

related by rotation along any of the $\{101\}_{Cst}$ planes for 50.3°. In cassiterite viewed along the $[101]_{Cst}$ zone axis, one pair of $\{101\}_{Cst}$ planes is edge-on oriented, these planes intersect at 67.8° [see stereogram in Fig. 5(a)] and limit the number of subsequent twin boundaries in coplanar cyclic twins of cassiterite to five. Along the $[111]_{Cst}$ zone axis, another pair of $\{101\}_{Cst}$ planes is edge-on oriented, these planes intersect at 46.5° [see stereogram in Fig. 5(d)] and limit the number of subsequent twin boundaries in alternating cyclic twins of cassiterite to seven (Padrón-Navarta et al., 2020). In $[111]_{Cst}$ zone axis, the unit-cell projection of cassiterite may be drawn by a squashed hexagon with $\{101\}$ planes as the longer diagonals. To study the role of $CoNb_2O_6$ and $Co_4Nb_2O_9$ in the formation of alternating twins, both structures are shown in orientations obtained by equivalent rotation as SnO_2. Rotation of $CoNb_2O_6$ along the $(002)_{Col-t}$ planes yields $CoNb_2O_6$ along the $[1\bar{3}0]_{Col-t}$ [Fig. 5(e)] whereas, after 51.7° rotation of $Co_4Nb_2O_9$ along the $[110]_{Crn-t}$ direction, the structure is oriented along the $[2\bar{2}1]_{Crn-t}$ zone axis.

3.3.2. Twinning in SnO_2 and its relation to the columbite-type $CoNb_2O_6$. Columbite-type $CoNb_2O_6$ is structure-similar to α-PbO_2, which is also the structural type of high p-T modification of rutile, TiO_2. It has been shown that $\{101\}$ twins of rutile, found as inclusions in garnets contain epitaxial α-PbO_2 modification of TiO_2 at the twin contact with the following OR: $[100]_{\alpha-TiO2} \parallel [100]_{Rt}$; $(001)_{\alpha-TiO2} \parallel (011)_{Rt}$ (Hwang et al., 2000; Meng et al., 2008). Wittkamper et al. (2017) studied the growth of SnO_2 on polished polycrystalline columbite-type $CoNb_2O_6$ substrate with random grain orientation by pulsed laser deposition at 700°C. They found that SnO_2 develops in two polymorphic modifications on substrate $CoNb_2O_6$ grains, as rutile-type or as α-PbO_2-type SnO_2 modification, depending on the orientation of the substrate $CoNb_2O_6$ grains. In grains that promoted the growth of rutile-type SnO_2, the following OR was determined between SnO_2 and $CoNb_2O_6$ (c*, columbite indexed by nonstandard $Pcnb$ space group): $(101)_{Cst}[010]_{Cst} \parallel (010)_{c*}[001]_{c*}$ The OR is identical to the OR between α-PbO_2-type TiO_2 and rutile TiO_2 in $\{101\}$ twins of rutile in garnets (Hwang et al., 2000; Meng et al., 2008).

Both findings support our assumption that columbite-type $CoNb_2O_6$ particles can act as seed grains for epitaxial growth of SnO_2 in the dual-doped ceramics. $CoNb_2O_6$ is the first secondary phase that forms between cobalt and niobium oxides during the firing of doped SnO_2-based ceramics already around 700°C [see Fig. 3(a)]. Wittkamper et al. (2017) have shown that SnO_2 grows epitaxially on columbite-type $CoNb_2O_6$ already at temperatures as low as 700°C. A similar process of epitaxial nucleation of SnO_2 on $CoNb_2O_6$ seed particles may occur in polycrystalline ceramics, where heterostructural nucleation of SnO_2 on $CoNb_2O_6$ seed in identical or in mirror orientation may be anticipated (Fig. 6). Nucleation in identical orientation results in the formation of normal (untwinned) cassiterite grains [Fig. 6(a)], whereas nucleation in mirror orientation results in the formation of a contact {101} twin [Fig. 6(b)]. Such composite heterostructural
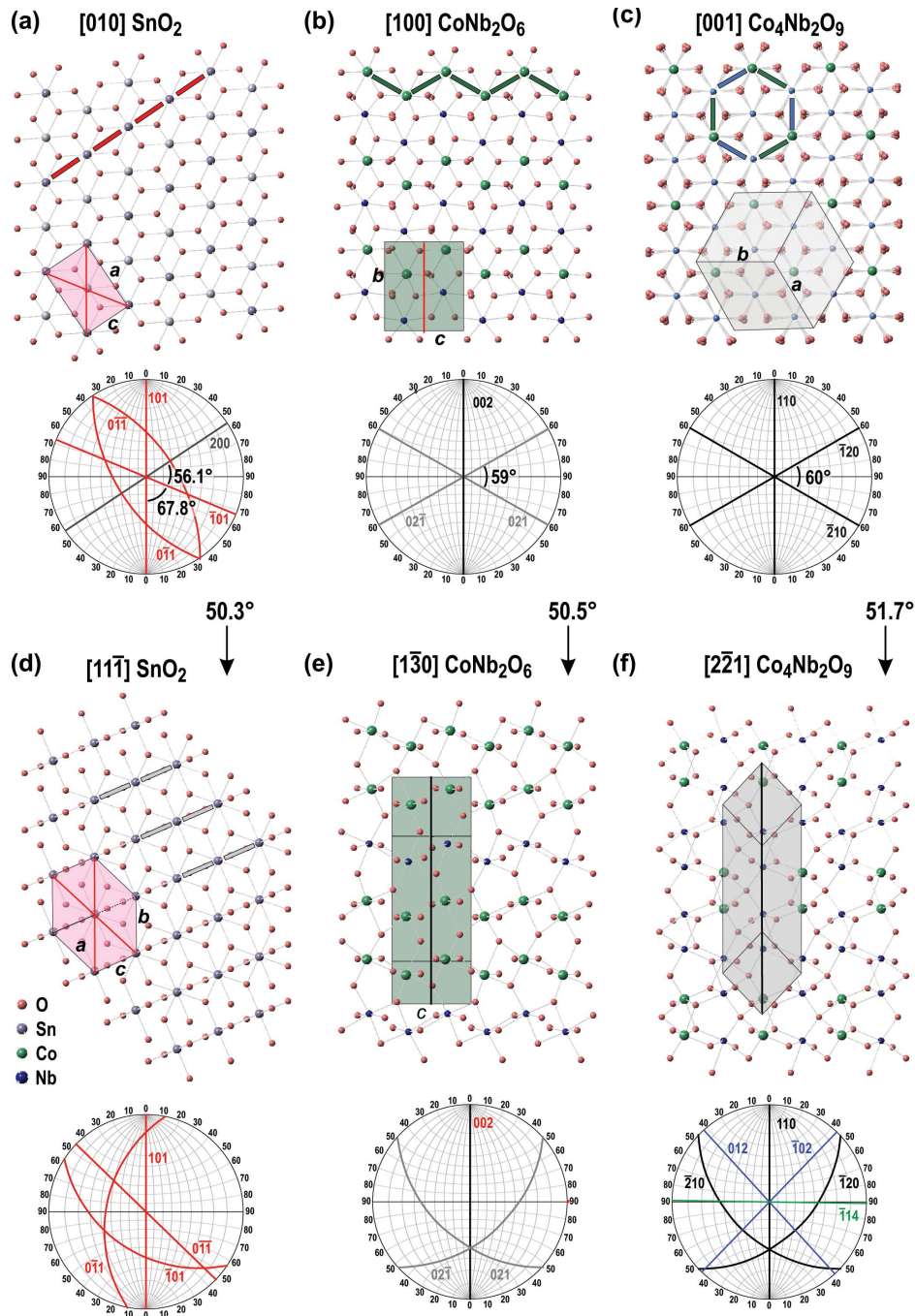
Figure 5
Structures of (a,d) SnO_2, (b,e) columbite-type $CoNb_2O_6$ and (c,f) $Co_4Nb_2O_9$ phase with structure coparable to that of corundum in orientations relevant for understanding the formation of (a)–(c) contact and (d)–(f) alternating cyclic twins in cassiterite by oriented growth of SnO_2 on the two structurally related phases. Typical pattern (projected unit cell) of each phase is drawn on the structural models and these patterns will be used for schematic illustration of epitaxial twinning in Figs. 6–8. A stereogram with the most relevant lattice planes involved in the twinning process is shown below each structural model.

Nina Daneu *et al.* • Multiple cyclic cassiterite twins in SnO_2-based ceramics **703**
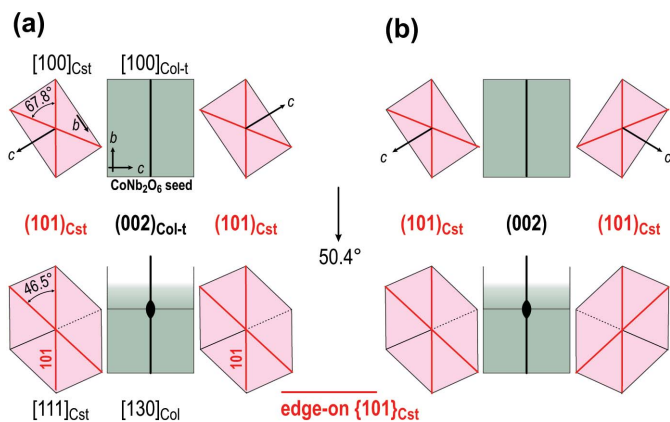
Figure 6
Oriented growth of SnO₂ (purple) on CoNb₂O₆ (greenish) seed can result in (a) identical orientation of SnO₂ on opposite sides of the CoNb₂O₆ seed particle leading to the formation of untwinned cassiterite or (b) in mirror orientation for the formation of contact (101) twin.

particles that are established at lower sintering temperatures represent nuclei for the development of SnO₂ contact twins during accelerated grain growth above 1300°C [see densification curve for the dual-doped ceramics in Fig. 1 (red curve) of Tominc *et al.* (2018)]. An additional effect that occurs in the high-temperature sintering stage is the reaction between CoNb₂O₆ and SnO₂. This causes dissolution of columbite seed grains into the cassiterite matrix grains and hence, the presence of secondary phase grains at the TBs or in the form of overgrown inclusions inside cassiterite grains is never observed. Our previous HR-STEM analyses of TBs and regions in the vicinity of the contacts have revealed non-uniform local enrichment with Co and Nb and also inhomogeneous distribution of both elements inside the SnO₂ matrix (Tominc *et al.*, 2018). This supports the hypothesis about epitaxial growth of SnO₂ on preexisting nanosized CoNb₂O₆

seeds and their later recrystallization and diffusion of Co²⁺ and Nb⁵⁺ into the cassiterite matrix.

3.3.3. Twinning in SnO₂ and its relation to the Co₄Nb₂O₉. In addition to the CoNb₂O₆ particles with the columbite-type structure, also the Co₄Nb₂O₆ phase grains with structure comparable to that of corundum can act as seed grains for the nucleation of cassiterite twins. The results of EBSD and TEM analyses have revealed that the following OR preferentially occurs between SnO₂ and Co₄Nb₂O₉: (101)[010]$_{Cst}$ ‖ (110)[001]$_{Crn-t}$ (Fig. 4). The small mismatch between (101)$_{Cst}$ and (110)$_{Crn-t}$ planes (Table 2) is advantageous for the development of this OR. Epitaxial growth of SnO₂ on Co₄Nb₂O₉ seed grains in this OR can follow 12 possible orientations as schematically shown in Fig. 7(*a*). Theoretically, any two SnO₂ domains that grow on a single crystal seed particle may form a (symmetric) interface. This results in 144 combinations, and the contacts can be classified into four types: (i) low-angle tilt boundaries at 7.8° and complementary angles of 172.2° (contacts 1–2 and analogous); (ii) non-crystallographic contacts at 60° and 120° (1–3, 1–5 and analogous), (iii) {101} TBs at 67.8° (contacts 1–4 and analogous) and (iv) {301} TBs at 127.8° (contacts 1–6 and analogous). Also, nucleation of cassiterite in identical orientation resulting in the formation of single-crystal cassiterite at 0° or 180° (the structure is centrosymmetric) may occur (1–1, 2–2...). The possibilities are schematically presented in Fig. 7(*b*); a more detailed description of this process is given in the description of rutile exsolutions from matrix ilmenite, FeTiO₃ [see Table 1 and the corresponding explanation given by Rečnik *et al.* (2015)].

Epitaxial growth of SnO₂ domains in various orientations on a Co₄Nb₂O₉ seed grain can result in the formation of different non-crystallographic and crystallographic contacts between SnO₂ domains. However, the only contact between cassiterite domains that we found in the dual-doped ceramics
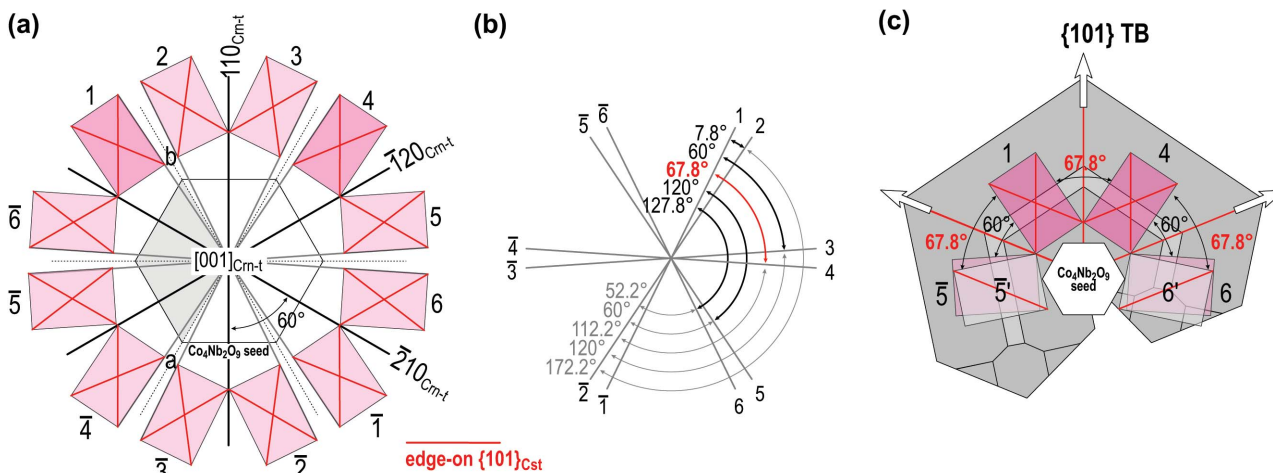
Figure 7
(*a*) Twelve possible (six unique) orientations of cassiterite (purple) in [010]$_{Cst}$ orientation on Co₄Nb₂O₉ seed (gray) in [001]$_{Crn-t}$ orientation. (*b*) Angles between *c* axes of the domains, at 67.6° angle, the domains are in (101) twin orientation. (*c*) Formation of domains 1 and 4 gives a contact twin. The formation of additional SnO₂ domains for a coplanar twin on the same seed grain requires epitaxial growth of SnO₂ at 60° (domains 6 and 5̄) and local recrystallization of these domains to 6′ and 5̄′ orientation to yield the (101) TB contacts.

(a)

(b)
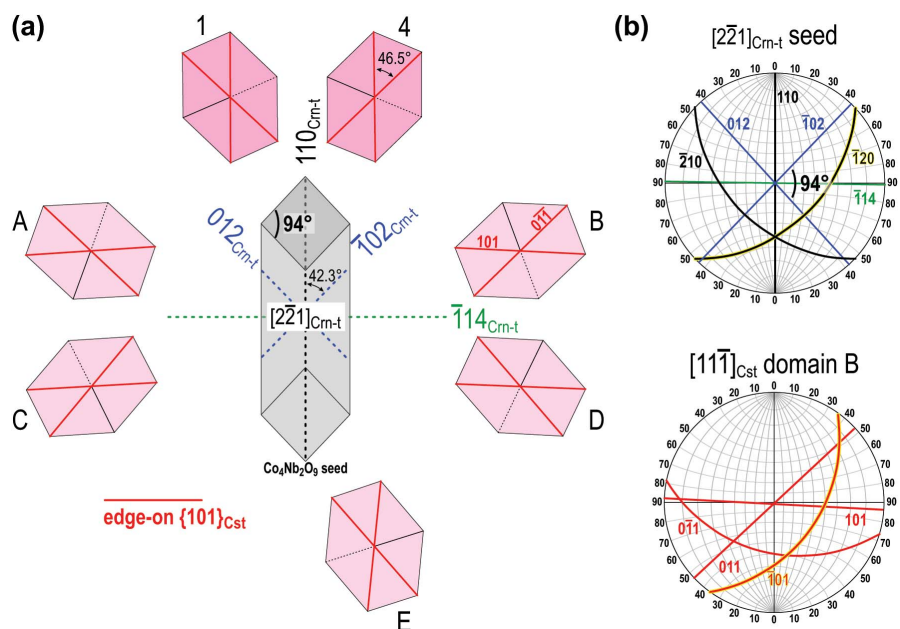
Figure 8
(a) Scheme of an alternating twin where all cassiterite domains are oriented along their $[111]_{Cst}$ zone axis and the $Co_4Nb_2O_9$ seed is oriented along the pseudo fourfold $[2\bar{2}1]_{Crn-t}$ zone axis. (b) Stereograms of the $Co_4Nb_2O_9$ seed and SnO_2 domain B show that besides the edge-on $(\bar{1}02)_{Crn-t}$ and $(0\bar{1}1)_{Cst}$ planes, another pair of planes $(\bar{1}20)_{Crn-t}$ and $(0\bar{1}1)_{Cst}$ lies oblique to the viewing direction (marked by yellow). This pair of planes corresponds to the expected SnO_2–$Co_4Nb_2O_9$ OR.

are crystallographic (101) TBs. This implies that this interface is the most energetically stable and develops/grows further after epitaxial growth of SnO_2 domains in twin orientation on the seed particle. We even assume that neighboring domains that form at angles close to the (101) TBs (*e.g.* 60°) may recrystallize to twin contacts at the beginning of grain growth. The energy of (101) and (301) twin boundaries with different local stacking was calculated for rutile, TiO_2 by Lee *et al.* (1993) and they found that reflection twin with $\frac{1}{2}\langle111\rangle$ in-plane translation is the lowest energy interface in rutile. Since TiO_2 and SnO_2 are isostructural, we may assume that (101) TBs are low-energy interfaces also in cassiterite. The prevalence of (101) TBs in our ceramics samples and also the abundance of (101) twins over (301) twins in natural cassiterite crystals are also in favor of this hypothesis. Epitaxial growth of cassiterite in {101} twin orientation on $Co_4Nb_2O_9$ seed can result in the formation of simple contact twins, *i.e.* between cassiterite domains 1–4, 2–5 or 3–6 in Fig. 7(*a*). Each of these simple contact twins may represent the basis for the development of a multiple cyclic twin with either coplanar or alternating configuration.

Let us now focus on the formation of coplanar multiple cyclic twins. In our samples, we observed grains with three or four domains although theoretically coplanar cyclic twins with six domains separated by five subsequent {101} TBs and an additional non-crystallographic contact to close the cyclic twin are possible (Padrón-Navarta *et al.*, 2020). Nucleation of a cyclic twin cannot be explained by epitaxial growth of SnO_2 domains in identical OR on a $Co_4Nb_2O_9$ seed. We believe that the formation of a coplanar cyclic twin starts with the

formation of a contact twin, for example between domains 1 and 4 [Fig. 7(*c*)]. The formation of additional domains on a single-crystal $Co_4Nb_2O_9$ seed grain in twin orientation with the domains 1 and 4 and, at the same time, in the expected OR between SnO_2 and $Co_4Nb_2O_9$ (with {101}$_{Cst}$ parallel to {110}$_{Crn-t}$) is not possible. The closest possibility is epitaxial growth of SnO_2 domains on $Co_4Nb_2O_9$ at 60° angles on both sides of the starting contact twin (domain $\bar{5}$ next to 1 and or domain 6 next to 4). These would initially form energetically demanding non-crystallographic contacts at 60°, which would then locally recrystallize to (101) twin contact (domain $\bar{5} \rightarrow \bar{5}'$ and $6 \rightarrow 6'$). Such occurrence on only one side of the 1–4 contact twin would lead to the formation of a coplanar twin with three domains, whereas the occurrence of the process on both sides of the starting 1–4 contact twin would lead to the formation of a coplanar twin with four domains separated by three TB contacts [*e.g.* domains $\bar{5}'$–1–4–6', Fig. 7(*c*)]. In any case, each cyclic twin is closed by the formation of a short NCC between the end domains [*e.g.* 5' and 6' in Fig. 7(*c*)].

Besides coplanar cyclic twins, a comparable fraction of alternating cyclic twins always forms in the ceramics (Padrón-Navarta *et al.*, 2020) indicating that the probability for the formation of coplanar and alternating twins is similar. We may presume that the initial structural element, *i.e.* a contact {101} twin on a $Co_4Nb_2O_9$ particle can also develop into an alternating multiple cyclic twin, where all twin domains have the $[111]_{Cst}$ as the common zone axis. In order to understand the crystallographic relationship between SnO_2 domains and the $Co_4Nb_2O_9$ seed, it is beneficial to study the phases in rotated view (Fig. 8). Fig. 8(*a*) is a scheme of alternating cassiterite twin with the maximum possible number of twin domains (*i.e.* seven) which are separated by six twin boundary contacts. In the dual-doped ceramics, twins with three or four subsequent domains are the most common, whereas twins with five or more domains are quite rare (Padrón-Navarta *et al.*, 2020). This suggests that conditions for the formation of a fully developed alternating twin of cassiterite in sintered ceramics are hardly ever achieved.

Cassiterite domains in Fig. 8(*a*) are oriented along their $[111]_{Cst}$ zone axes, whereas the seed is in the $[2\bar{2}1]_{Crn-t}$ orientation. Cassiterite domains 1 and 4 and the $Co_4Nb_2O_9$ seed represent the basic element for the development of twins with coplanar [Fig. 7(*a*)] or alternating morphology. Here, the OR between cassiterite domains 1 and 4 and the seed can alternatively be written as $(101)[111]_{Cst} \parallel (110)[2\bar{2}1]_{Crn-t}$ (see also Figs. 4, 5(*d*) and 5(*f*)). A common characteristic of all other cassiterite domains (marked by letters A-E) is that they have

one of the oblique $(101)_{Cst}$ lattice planes nearly parallel to one of the oblique $(110)_{Crn-t}$ planes of the $Co_4Nb_2O_9$ seed, which corresponds to the expected SnO_2–$Co_4Nb_2O_9$ OR; an example for SnO_2 domain B and the $Co_4Nb_2O_9$ seed is shown on the stereograms in Fig. 8(b). This OR between cassiterite and corundum may lead to the stabilization of (101) TBs between cassiterite domain B and domain 1 as the low-energy interface and subsequent recrystallization to a cyclic twin with alternating morphology. It is also interesting that in this orientation, the corundum-type structure exhibits pseudo-cubic symmetry with $(110)_{Crn-t}$ planes (d = 0.2587 nm) nearly perpendicular to $(\bar{1}14)_{Crn-t}$ planes (d = 0.2776 nm), whcih coincides with the pseudo eightfold symmetry of the alternating twin and may additionally contribute to the stabilization of cyclic twins with alternating morphology.

3.4. Microstructure development and the formation of different types of twins in SnO_2-based ceramics co-doped with cobalt and niobium oxides

The main goal of this work was to understand the formation of contact and multiple cyclic twins of cassiterite which commonly form when in SnO_2-based ceramics when SnO_2 is sintered with small additions of CoO and Nb_2O_5 (1 mol% of each dopant; Co:Nb = 1:2). Exactly this composition, in terms of the total amount of the dopants and the Co:Nb ratio, yields microstructure with the highest density, composed of large SnO_2 grains with a high fraction of twins (Tominc *et al.*, 2018). The microstructure contains about two thirds of untwinned grains and the rest are cassiterite twins, most of which are contact (101) twins, while about 6% of all grains are multiple cyclic twins with coplanar or alternating morphologies that occur in comparable fractions (Padrón-Navarta *et al.*, 2020). The fact that abundant twinning and especially the formation of multiple cyclic twins is not observed in the samples without the addition of both dopants implies that twinning in the dual-doped cassiterite is related to a combination of specific chemical and thermodynamic conditions during the high-temperature sintering of SnO_2 in the presence of both oxides.

It has been observed in several oxides and alloys that the addition of specific dopants/ impurities triggers the formation of crystallographic contacts like twin boundaries and similar interfaces during grain/crystal growth. For example, the formation of growth twins on {111} planes is observed in silicon flakes during their growth in aluminium–silicon eutectic alloy as a result of the addition of sodium and other modifiers (Lu & Hellawell, 1987); the formation of basal-plane inversion boundaries (IBs) in ZnO is triggered by the addition of Sb_2O_3, SnO_2, and other oxides (Rečnik *et al.*, 2001a; Daneu *et al.*, 2000; Schmid *et al.*, 2013), abundant formation of {111} twins in $MgAl_2O_4$ spinel is observed during crystal growth in the presence of BeO (Drev *et al.*, 2013) antiphase boundaries typically form in non-stoichiometric or doped oxide perovskites (*e.g.* Rečnik *et al.*, 2001b). Characteristic of these impurity-induced planar defects is enrichment of the interface with the dopant atoms and these atoms reside in specific interstitial positions within the boundary. The local atomic structure of these interfaces is well ordered and contains structural elements found in the secondary phase that forms between the main phase and the dopant, *i.e.* spinel phases in the case of IBs in ZnO, taaffeite modulated phase in the case of twins in BeO-doped $MgAl_2O_4$ spinel and polytypic Ruddlesden–Popper phases in the case of antiphase boundaries in perovskites. The formation of impurity-induced planar defects is an energetically favorable process and can be described as continuous adsorption of impurity atoms to the growth interface which results in the progressive formation of a 2D monolayer with different chemical compositions inside the host crystal (Lu & Hellawell, 1987). The process has a profound effect on grain/crystal growth and the development of ceramic microstructures. Grains in which the impurity-induced interfaces nucleate at the beginning of crystal growth exhibit exaggerated growth, their growth is significantly faster in the direction of the defect and these grains may also develop anisotropic morphologies, at least in the initial stages of crystal growth.

If the twin boundaries in co-doped cassiterite that we studied in this work would be classic impurity-induced defects, we would expect to find Co and/or Nb ordered inside the twin contact planes. However, the results of our previous study (Tominc *et al.*, 2018) have shown that the twin boundaries in co-doped cassiterite contain only irregular segregation of Co and Nb to the vicinity of the twin boundaries, while an ordered arrangement of the dopants within the interface was not observed. Also, these twin boundaries do not show exaggerated growth to such extent as observed in the systems with the impurity-induced defects and this suggests that these defects form via a different mechanism. An important clue for understanding the formation of twins in co-doped cassiterite ceramics is the crystallographic relationship between SnO_2 and the $Co_4Nb_2O_9$ secondary phase: $(101)[010]_{Cst}$ $\parallel$ $(110)[001]_{Crn-t}$ that was found in the sample with higher dopant additions (Fig. 4). In natural rutile twins, the twin boundaries sometimes contain up to few nanometres thick layers or inclusion of structurally related phases that indicate the formation of these twins is by epitaxial growth on structurally related phases or by oriented (topotaxial) recrystallization of a structurally related precursor mineral. For example, a thin epitaxial layer of ilmenite was found at (301) rutile twin contacts (Daneu *et al.*, 2007), whereas discrete oriented corundum-inclusions were found at (101) twin boundaries (Daneu *et al.*, 2014), both in hydrothermally formed rutile crystals. On the other hand, (101) twins of rutile found as inclusions in high *P-T* garnets contain a nanometre-thick slab of α-PbO_2-type TiO_2 at the interface (Hwang *et al.*, 2000; Meng *et al.*, 2008). Structural characteristics of epitaxial secondary phases found at the twin contacts are important indicators of geochemical conditions during the rutile crystal growth/formation.

The results of our study suggest that twins in co-doped cassiterite ceramics form according to a similar mechanism that involves oriented epitaxial growth of SnO_2 domains on grains of secondary $CoNb_2O_6$ and $Co_4Nb_2O_9$ phases. These particles represent heterogeneities in the system, which act as

seeds and lower the energy barrier for epitaxial growth of SnO_2 (Lee *et al.*, 2016). The structural similarities between SnO_2 and both secondary phases favor the formation of heterointerfaces. The presence of seed grains is overwritten during the high-temperature sintering when solid-state diffusion processes that govern coarsening of cassiterite grains (twin growth stage) become activated. The only (indirect) evidence for the presence of seed grains that trigger the nucleation of twins in the initial stages of crystal growth is irregular segregation of Co and Nb to the twin boundaries (Tominc *et al.*, 2018) and local enrichment of the cyclic twin cores as shown in this work [Fig. 2(*c*)]. The process is presented in Fig. 9 and described in more detail in the continuation.

The starting pellet contains mostly nanosized SnO_2 powder homogenized with the addition of 1 mol% of CoO and 1 mol% of Nb_2O_5 (Co:Nb ratio of 1:2). The distribution of both dopants in the starting pellet is not perfectly homogenous and areas with locally higher concentrations of cobalt oxide (with larger particles in the starting powder) are likely [Fig. 9(*a*)]. The first reaction that occurs during the heating is the formation of the $CoNb_2O_6$ phase at around 700°C. Due to the close structural relationship between $CoNb_2O_6$ and SnO_2, the SnO_2 grain in the vicinity of the $CoNb_2O_6$ phase grains can locally recrystallize onto these grains in the orientation for (101) twins [Fig. 9(*b*)]. The formation of $Co_4Nb_2O_9$ phase starts at around 900°C in areas locally enriched with cobalt oxide with the reaction between $CoNb_2O_6$ and excess cobalt oxide. These particles represent seeds for the formation of contact and multiple cyclic twins [Fig. 9(*c*)]. In the temperature range up to 1300°C, densification of the sample is very limited, the sample behaves similarly to undoped SnO_2, where sintering in the low-temperature range (500–1000°C) is controlled by surface diffusion, and shrinking is not observed (Leite *et al.*, 2001). The only processes observed in this temperature range are reactions between cobalt and niobium oxides to $CoNb_2O_6$ and $Co_4Nb_2O_9$ secondary phases and these reactions do not have an influence on the densification. The secondary phase particles, however, represent seeds for local recrystallization of SnO_2, which results in the formation of twin nuclei for the grwoth of different types of twins at higher sintering temperatures. The genesis of twins in the nucleation stage as a result of the presence of impurities has been suggested already by Senechal (1980).
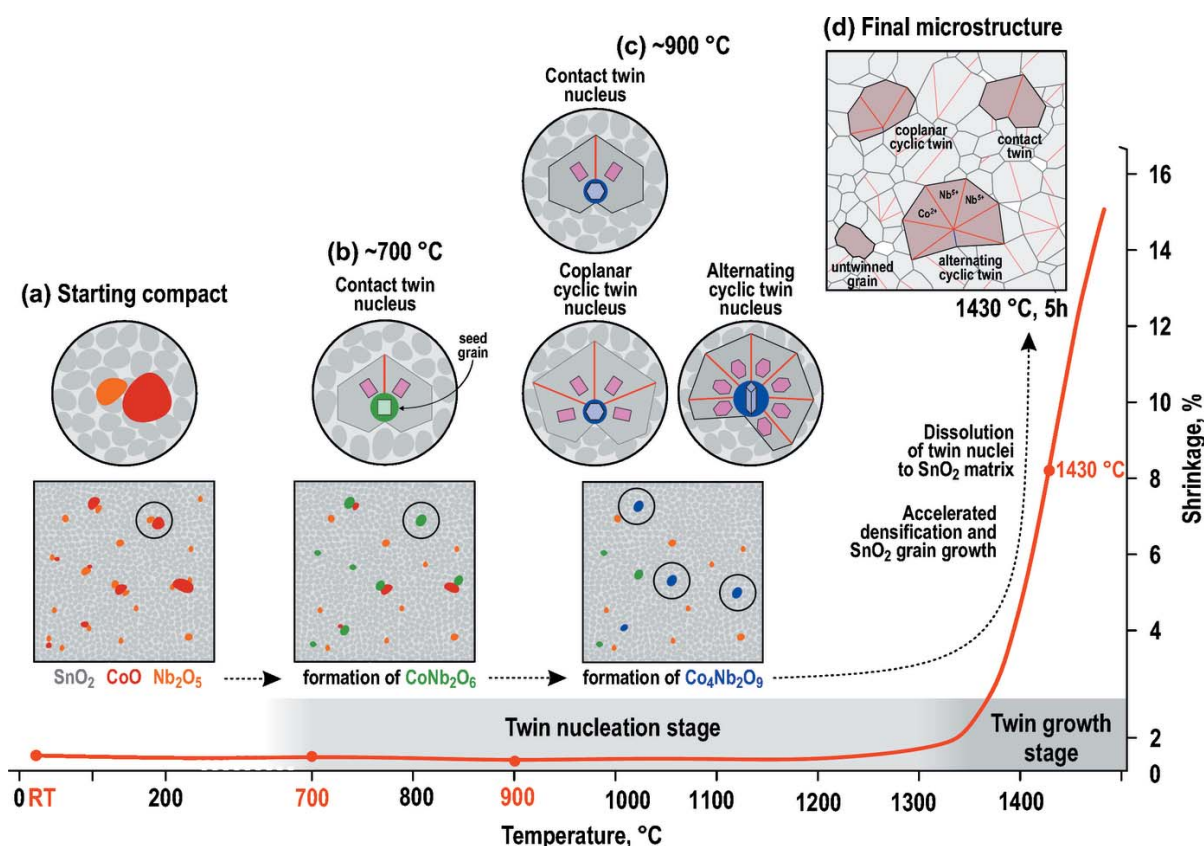

Figure 9
The formation of different types of twins in dual-doped SnO_2 during heating up to 1430°C; red line is the sample densification curve according to Tominc *et al.* (2018). (*a*) Inhomogeneous distribution of the dopants (CoO, red; Nb_2O_5, orange) among nanosized SnO_2 (gray) particles the starting compact. (*b*) The formation of $CoNb_2O_6$ seed particles (green) and contact twins nuclei at around 700°C and (*c*) the formation of $Co_4Nb_2O_9$ seeds (purple) and contact and multiple cyclic twins nuclei at around 900°C. (*b*) and (*c*) represent the twin nucleation stage, which is bound to limited densification at temperatures up to ~1300°C. (*d*) The twin growth stage coincides with accelerated densification and SnO_2 grain growth above 1300°C. During this stage, the twin nuclei develop into cassiterite twins due to the fast growth of (101) twin contacts. The seed grains recrystallize to SnO_2, Co^{2+} and Nb^{5+} are incorporated into SnO_2 grains in the form of solid solution and seed grains are no longer present at the TBs and in the cyclic twin cores in the form of crystalline particles.

At temperatures above 1300°C, densification of the sample is strongly enhanced [Fig. 9(d)]. It is related to accelerated solid-state diffusion due to the formation of point defects as a result of aliovalent doping as described by Tominc *et al.* (2018). During these processes, Co and Nb are incorporated into the SnO_2 matrix in the form of solid solution. The total addition of CoO and Nb_2O_5 in the low-doped sample (1 mol% of each dopant) is around or below the solid solubility limit of the dopants in SnO_2 matrix (our estimated value of total Co and Nb solid solubility in SnO_2 is ~6 at%), therefore almost all dopants are incorporated into the SnO_2 in the low-doped sample. The columbite-type $CoNb_2O_6$ phase grains will in any case react with the SnO_2 to the trirutile phase above 1200°C, therefore these grains, which represent the nuclei for contact twins readily dissolve into SnO_2. This explains the local enrichment in Co and Nb around the twin boundaries as observed in our previous work (Tominc *et al.*, 2018). Dissolution of the $Co_4Nb_2O_9$ grains into the SnO_2 matrix phase along with the formation of secondary Co_2SnO_4 spinel phase particles in the reaction between excess cobalt oxide and SnO_2 can also occur in the low-doped samples, where the total dopant addition does not exceed the solid solubility limit. In our previous study we found some residual niobium oxide and Co_2SnO_4 spinel phase particles at the grain boundaries and triple points. Both can be attributed to imperfect homogenization of the starting powders and limited diffusion during solid-state sintering. The development of cyclic twins with eccentrically positioned nuclei with long TBs and a short NCC between the first and the last twin domain is a result of the fast growth of low-energy (101) TB contacts and very limited growth of the energetically unfavorable NCC.

The described sequence of chemical reactions and epitaxial growth processes not only offers a plausible explanation for the formation of contact and multiple cyclic twins by the 'epitaxially induced twinning' mechanism during the sintering of dual-doped SnO_2-based ceramics, but also explains the presence of untwinned grains, which represent two-thirds of all grains. Untwinned grains may simply coarsen without an epitaxial contact to a secondary cobalt–niobium oxide grain, by epitaxial growth of a single SnO_2 domain on a seed, by the growth of two or more SnO_2 domains in identical or inconvenient orientation for the formation of a (101) twin contact on a seed particle. It is also important to emphasize that higher dopant additions do not enhance the formation of twins because we found many untwinned grains also in the sample with much higher addition of both dopants [see Fig. 4(a)]. Even more interesting, this sample contained fewer multiple cyclic twins in comparison to the low-doped sample, and twins with maximum four twin domains were observed. This suggests that small, nanosized nuclei are necessary for the formation of multiple cyclic twins.

4. Conclusions

The results of this study indicate that the formation of contact and multiple cyclic twins in SnO_2-based ceramics co-doped with cobalt and niobium oxides is not accidental but triggered by oriented growth of SnO_2 domains in twin orientations on structurally related nanosized seed particles of secondary phases via the so-called 'epitaxially-induced twinning' mechanism.

The formation of twins is a two-stage process. The twin nuclei form in the twin nucleation stage below 1300°C, where only local recrystallization of SnO_2 on $CoNb_2O_6$ and $Co_4Nb_2O_9$ seed particles occurs. These particles have crystal structures closely related to SnO_2 and enhance the formation of heteroepitaxial contacts with SnO_2 domains in different orientations. In the twin nucleation stage, some of the SnO_2 domains are in (101) twin orientation and contacts between these domains develop into (101) TBs. These TBs then grow preferentially in the twin growth stage above 1300°C, when densification and SnO_2 grain growth are strongly accelerated as a result of diffusion processes related to the incorporation of Co and Nb into the SnO_2 matrix. This stage involves recrystallization/dissolution of the seed grains into the matrix SnO_2 and obliterates the evidence about the twin nucleation stage.

One of the most important implications of this study is that the absence of a twin nucleus in a growth twin does not necessarily imply that it was not present in the twin nucleation stage. Detailed analyses of the twin contacts and twin cores, especially in the case of multiple cyclic twins provide valuable evidence about the presence of seed particles in the nucleation stage of the twin formation.

References

Armbruster, T. (1981). *N. Jahrb. Miner.* **7**, 328–334.
Aruga, A., Tokizaki, E., Nakai, I. & Sugitani, Y. (1985). *Acta Cryst.* C**41**, 663–665.
Baur, W. H. (1981). *Mater. Res. Bull.* **16**, 339–345.
Beck, H. P. (2012). *Z. Kristallogr. Cryst. Mater.* **227**, 843–858.
Bertaut, E. F., Corliss, L., Forrat, F., Aleonard, R. & Pauthenet, R. (1961). *J. Phys. Chem. Solids*, **21**, 234–251.
Castellanos, R. M. A., Bernès, S. & Vega-González, M. (2006). *Acta Cryst.* E**62**, 117–119.
Daneu, N., Rečnik, A., Bernik, S. & Kolar, D. (2000). *J. Am. Ceram. Soc.* **83**, 3165–3171.
Daneu, N., Rečnik, A. & Mader, W. (2014). *Am. Mineral.* **99**, 612–624.
Daneu, N., Schmid, H., Rečnik, A. & Mader, W. (2007). *Am. Mineral.* **92**, 1789–1799.
Drev, S., Rečnik, A. & Daneu, N. (2013). *CrystEngComm*, **15**, 2640.

Force, E. R., Richards, R. P., Scott, K. M., Valentine, P. C. & Fishman, N. S. (1996). *Can. Mineral.* **34**, 605–614.

Goldschmidt, H. J. (1960). *Metallurgia*, **62**, 211–218.

Grimmer, H. (1979). *Scr. Metall.* **13**, 161–164.

Hahn, Th. & Klapper, H. (2006). *International Tables for Crystallography*, Vol. D, *Physical properties of crystals*, edited by A. Authier, ch. 3.3, pp. 393–448. Dordrecht: Kluwer.

Hielscher, R. & Schaeben, H. (2008). *J. Appl. Cryst.* **41**, 1024–1037.

Hwang, S. L., Shen, P., Chu, H. T. & Yui, T. F. (2000). *Science*, **288**, 321–324.

Kawamura, F., Kamei, M., Yasui, I. & Sunagawa, I. (1999). *J. Am. Ceram. Soc.* **82**, 774–776.

Krakow, R., Bennett, R. J., Johnstone, D. N., Vukmanovic, Z., Solano-Alvarez, W., Lainé, S. J., Einsle, J. F., Midgley, P. A., Rae, C. M. F. & Hielscher, R. (2017). *Proc. R. Soc. A*, **473**, 20170274.

Lee, J., Yang, J., Kwon, S. G. & Hyeon, T. (2016). *Nat. Rev. Mater.* **1**, 16034.

Lee, W. E. & Lagerlof, P. D. (1985). *J. Elec. Microsc. Tech.* **2**, 247–258.

Lee, W. Y., Bristowe, P. D., Gao, Y. & Merkle, K. L. (1993). *Philos. Mag. Lett.* **68**, 309–314.

Leite, E. R., Cerri, J. A., Longo, E., Varela, J. A. & Paskocima, C. A. (2001). *J. Eur. Ceram. Soc.* **21**, 669–675.

Lu, S. & Hellawell, A. (1987). *Metall. Trans. A*, **18**, 1721–1733.

Mainprice, D., Bachmann, F., Hielscher, R. & Schaeben, H. (2015). *Geol. Soc. London Spec. Publ.* **409**, 251–271.

Meng, D. W., Wu, X. L., Sun, F., Huang, L. W., Liu, F., Han, Y. J., Zheng, J. P., Meng, X. & Mason, R. (2008). *Micron*, **39**, 280–286.

Morawiec, A. (1997). *Acta Cryst.* A**53**, 273–285.

Navrotsky, A., Ma, C., Lilova, K. & Birkner, N. (2010). *Science*, **330**, 199–201.

Otálora, F. & García-Ruiz, J. M. (2014). *Chem. Soc. Rev.* **43**, 2013–2026.

Padrón-Navarta, J. A., Barou, F. & Daneu, N. (2020). *Acta Cryst.* B**76**, 875–883.

Pan, X. Q. & Fu, L. (2001). *J. Appl. Phys.* **89**, 6048–6055.

Penn, R. L. & Banfield, J. F. (1998). *Science*, **281**, 969–971.

Rečnik, A., Čeh, M. & Kolar, D. (2001*b*). *J. Eur. Ceram. Soc.* **21**, 2117–2121.

Rečnik, A., Daneu, N., Walther, T. & Mader, W. (2001*a*). *J. Am. Ceram. Soc.* **84**, 2657–2668.

Rečnik, A., Stanković, N. & Daneu, N. (2015). *Contrib. Mineral. Petrol.* **169**, 19.

Schmid, H., Okunishi, E. & Mader, W. (2013). *Ultramicroscopy*, **127**, 76–84.

Senechal, M. (1980). *Sov. Phys. Crystallogr.* **25**, 520–524.

Shahani, A. J. & Voorhees, P. W. (2016). *J. Mater. Res.* **31**, 2936–2947.

Stanković, N., Rečnik, A. & Daneu, N. (2016). *J. Mater. Sci.* **51**, 958–968.

Suzuki, K., Ichihara, M. & Takeuchi, S. (1991). *Philos. Mag.* **63**, 657–665.

Tominc, S., Rečnik, A., Samardžija, Z., Dražić, G., Podlogar, M., Bernik, S. & Daneu, N. (2018). *Ceram. Int.* **44**, 1603–1613.

Weitzel, H. (1976). *Z. Kristallogr.* **144**, 238–258.

West, A. R. & Bruce, P. G. (1982). *Acta Cryst.* B**38**, 1891–1896.

Whitney, D. L. & Evans, B. W. (2010). *Am. Mineral.* **95**, 185–187.

Wittkamper, J., Xu, Z., Kombaiah, B., Ram, F., De Graef, M., Kitchin, J. R., Rohrer, G. S. & Salvador, P. A. (2017). *Cryst. Growth Des.* **17**, 3929–3939.

Zheng, G., Pan, X. Q., Schweizer, M., Zhou, F., Weimar, U., Göpel, W. & Rühle, M. (1996). *J. Appl. Phys.* **79**, 7688–7694.